separations

*Article*

# Numerical Simulation of Critical Production Pressure Drop of Injection and Production Wells in Gas Storage Based on Gas-Solid Coupling

**Yiyong Sui [1,*], Mengying Luo [1], Tangmao Lin [2], Guihua Liu [3], Yuan Zhao [4], Yazhou Wu [5] and Lanqing Ren [1]**

[1] School of Petroleum Engineering, China University of Petroleum (East China), Qingdao 266580, China
[2] Sinopec Dalian Research Institute of Petroleum and Petrochemicals, Dalian 116000, China
[3] Geosteering & Logging Research Institute, Sinopec Dalian Research Institute of Petroleum and Petrochemicals Matrix Corporation, Qingdao 266000, China
[4] Tianjin Branch of CNPC Logging, Tianjin 300270, China
[5] Shengli Oilfield Dongsheng Jingtao Petroleum Development Group Co., Ltd., Dongying 257000, China
* Correspondence: suiyy@126.com; Tel.: +86-137-0636-8339

**Abstract:** The periodic injection-production process of natural gas in underground gas storage make the rock bear alternating load under the gas-solid coupling. The alternating load changes the physical properties of rock, and then influence the critical production pressure drop of injection-production wells in gas storage. In the case of gas-solid coupling, the decisive factors affecting the alternating load are the number of injection-production cycles and the injection-production differential pressure. Therefore, a discrete element numerical simulation model is established to simulate the gas-solid coupling process of gas storage wells under different injection-production cycle and differential pressure. The influence mechanism of injection-production cycle and differential pressure on particle cementation and primary crack is analyzed microscopically and also the influence law of injection-production cycle and differential pressure on rock mechanical properties is analyzed from the macroscopic. Finally, the influence law of injection-production cycle and differential pressure on the critical production pressure drop of injection-production wells due to gas-solid coupling can be obtained. The results show that under the influence of gas-solid coupling, the number of bonded contact cracks and micro cracks in the model increase gradually, both the elastic modulus ratio and the cohesion ratio decrease gradually with the increase of injection-production cycle and the higher the injection-production differential pressure, the greater the decline range. Then, with the injection-production cycle increasing the Poisson's ratio increases gradually and the higher the injection-production differential pressure, the greater the increase range. Finally, the internal friction angle ratio increases greatly in the initial stage, after that decreases and then shows a linear increase. According to the influence law, the relationship model between the critical production pressure drop of injection-production wells in gas storage and the injection-production cycle and differential pressure under the gas-solid coupling will be established, which is used for the dynamic prediction of the critical production pressure drop of injection-production wells in the whole life cycle of gas storage.

**Keywords:** gas-solid coupling; numerical simulation; modeling; injection-production differential pressure



**Citation:** Sui, Y.; Luo, M.; Lin, T.; Liu, G.; Zhao, Y.; Wu, Y.; Ren, L. Numerical Simulation of Critical Production Pressure Drop of Injection and Production Wells in Gas Storage Based on Gas-Solid Coupling. *Separations* **2022**, *9*, 305. https://doi.org/10.3390/separations9100305

Academic Editors: Liming Zhang and Kai Zhang

Received: 7 September 2022
Accepted: 10 October 2022
Published: 13 October 2022



## 1. Introduction

With the rapid development of natural gas market, underground gas storage has become an important part of peak shaving of natural gas supply, while gas storage in depleted oil and gas reservoirs is the most commonly used type of gas storage at present, and its working mode is periodic large-flow strong injection and strong production, but the construction and operation of gas storage are still in the primary stage [1–5].

Many scholars have studied the prediction of critical production pressure drop from the micro and macro perspectives of rocks and have made certain achievements. Li et al. [6] analyzed the development of horizontal cracks, the filling and cementation degree of cracks, the distribution of UCS along the wellbore and the influence of well completion fluid bubble invasion in cracked carbonate reservoirs, and established a critical production pressure drop prediction model. Erarslan [7] studied the structural characteristics of crack surface in the crack generation area in the rock from the micro point of view, and analyzed the variation law of macro mechanical properties of the rock. Oluyemi et al. [8] found the nonlinear character of rock failure envelope in oil and gas reservoirs based on a large number of experimental analysis. Based on Hoek-Brown failure criterion, a prediction model of critical production pressure drop of oil and gas wells suitable for damaged reservoirs was established. Adeyanju et al. [9] modified Griffitti rock failure criterion using McClintock and Walsh hypothesis and proposed a method for predicting the current critical production pressure drop of oil and gas wells by using commonly available reservoir rock mechanics parameters. Ge Xiurun et al. [10] made a triaxial loading test equipment matched with CT scanner to analyze the meso-structure evolution characteristics of rock fatigue damage under cyclic loading in real time. Nguyen et al. [11] combined the discrete element numerical method and fatigue damage model to study the fatigue damage characteristics of cemented materials.

According to the research results of the above scholars, the prediction of critical production pressure drop mainly focuses on static prediction and uses rock mechanics parameters which only represent reservoir physical properties at the initial stage of development to predict critical production pressure drop without considering the influence of dynamic changes of reservoir rock mechanics parameters with the production process under the action of gas-solid coupling on critical production pressure drop, which leads to the fact that the critical production pressure drop of injection-production wells predicted by static model will not be applied to the whole life cycle of gas storage and has poor applicability. On the other hand, considering that the fatigue damage of rock under gas-solid coupling will affect the microstructure characteristics and macroscopic mechanical properties, it is necessary to use CT and other technologies to analyze the internal structure changes of rock. However, compared with numerical simulation methods, CT and other technologies have higher cost in large sample test and less research on fatigue damage of formation rock under gas storage operation mode.

Reasonable production pressure drop of injection-production wells is one of the key factors to ensure the safe production of gas storage [12–14]. Therefore, it is necessary to use numerical simulation method to build a numerical model to study the variation law of reservoir rock mechanical parameters with the increase of injection-production cycle under gas-solid coupling from micro and macro levels, modify the existing prediction model of critical production pressure drop of oil and gas wells, and establish a prediction model of critical production pressure drop of injection-production wells suitable for the production and operation mode of gas storage to ensure the safe and efficient operation of gas storage and injection-production wells.

## 2. Discrete Element Numerical Simulation Model and Experimental Conditions

As shown in Figure 1a, the size of true triaxial numerical model of core sample is 2.5 cm × 2.5 cm × 5 cm. The particle radius range is 0.27–0.74 mm, the model porosity is 0.3, and the model particle density is 2550 kg·m$^{-3}$. Creating crack network in particle system model to simulate the original crack of core sample. In the discrete element model of particle flow, discs with a certain size are used to simulate cracks [15–17]. According to the size of the numerical model, the size range of crack diameter is 0.7–1.2 cm, and the number of cracks is 180. The complex crack network model created is shown in Figure 1b. The complex crack network model is embedded into the particle system model. Figure 1c is the established core sample complex crack network particle model.

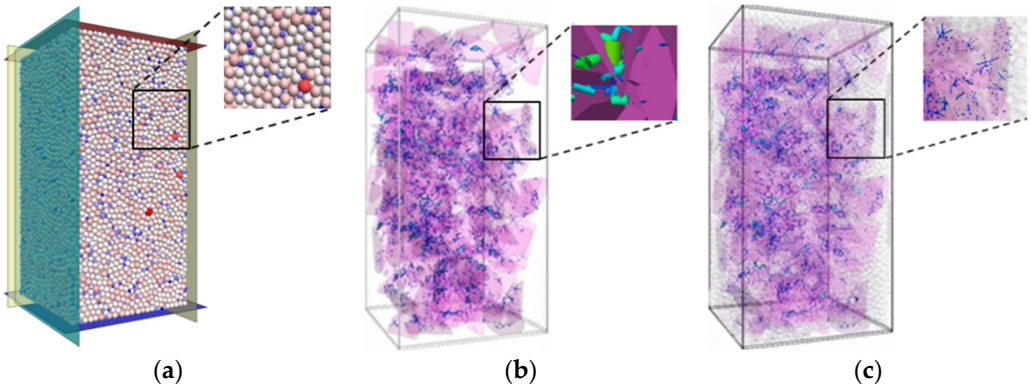

(**a**) (**b**) (**c**)

**Figure 1.** Particle model of complex crack network for core sample. (**a**) Granular system. (**b**) Crack network. (**c**) Numerical core.

In order to make the macroscopic mechanical properties of numerical core similar to that of actual core sample, linear parallel bond model is selected for the contact between particles in core particle system, and smooth joint model is used for complex crack network passing through the contact between particles. As shown in Figure 2, numerical simulation experiments of true triaxial compression under confining pressures of 10 MPa, 20 Mpa and 30 Mpa are carried out by setting contact parameters. Based on the principle that the elastic modulus, compressive strength and Poisson's ratio obtained from the actual core experiment and the numerical simulation experiment are consistent, the initial elastic modulus of the numerical core is determined to be 10,012 Mpa, the initial Poisson's ratio in the horizontal minimum and maximum principal stress directions is 0.2616 and 0.2237, respectively. The initial cohesive force is 12.631 Mpa and the initial internal friction angle is 38.39. The contact parameter values of the contact model are shown in Table 1.

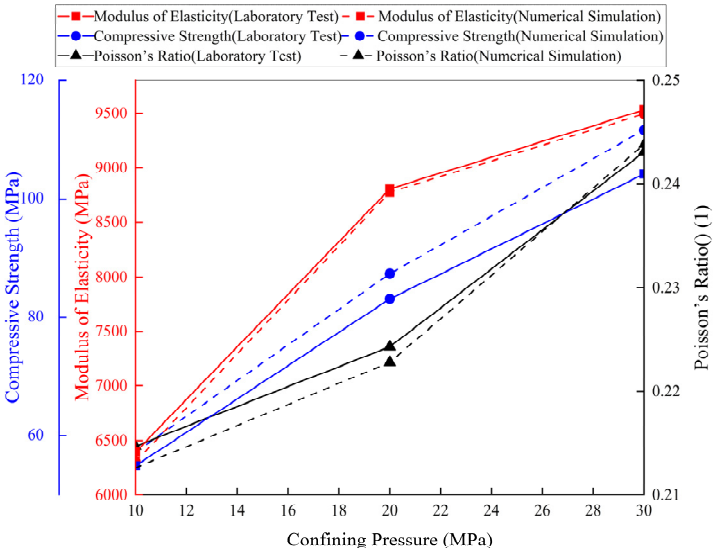


**Figure 2.** Comparison between numerical simulation results and laboratory test results.

**Table 1.** Linear parallel and smooth joint bond contact parameter values.

| Contact Parameter | Linear Parallel Bond | | | | | | | | Smooth Joint | | | | |
|---|---|---|---|---|---|---|---|---|---|---|---|---|---|
| | $\mu$ | E | $k_n/k_s$ | $\varphi$ (°) | $\bar{E}$ (Gpa) | $\bar{k}_n/\bar{k}_s$ | $\bar{\sigma}_c$ (Mpa) | $\bar{\tau}_c$ (Mpa) | $\mu_s$ | $k_n$ ($N \cdot m^{-1}$) | $k_s$ ($N \cdot m^{-1}$) | $\sigma_c$ (MPa) | $\tau_c$ (MPa) |
| Values | 0.5 | 5.0 | 7.0 | 40 | 9.2 | 7.0 | 12.0 | 10.0 | 0.35 | $2 \times 10^9$ | $2 \times 10^9$ | 0.5 | 1.0 |

The operation mode of the gas storage is periodic injection and production. The formation pressure changes during the injection-production process, resulting in the formation rock bearing the alternating load. Therefore, the multi periodic alternating load experiment is carried out on the numerical core by the particle flow discrete element numerical simulation method and the effects of injection-production cycle and differential pressure on the microstructure of core samples are studied from the microscopic point of view. In addition, the numerical simulation experiment of constant confining pressure axial alternating load loading is carried out on the core, and the confining pressures in the direction of horizontal maximum and minimum principal stress are set to be 38 Mpa and 26 Mpa, respectively. Firstly, the confining pressure is applied to the two horizontal principal stress directions by using the servo control principle of lateral boundary wall, and the confining pressure is kept constant in the process of simulation calculation. Then, setting the upper and lower limits of axial alternating load to 76 Mpa and 60 Mpa, respectively. At this time, the injection-production differential pressure is 16 Mpa. In addition, set the injection-production differential pressure to 18 Mpa, 20 Mpa, 22 Mpa, 24 Mpa, 26 Mpa, and 28 Mpa, respectively. The axial alternating load is loaded in the form of triangular wave. Finally, according to the production and operation life of the gas storage, the core is loaded for 60 cycles, as shown in Figure 3.

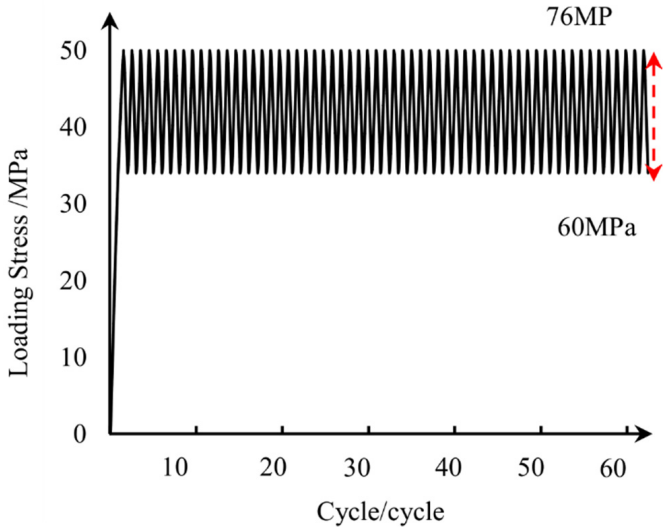


**Figure 3.** Cyclic stress loading diagram.

## 3. Results

### *3.1. Influence of Gas-Solid Coupling on Microstructure Change*

#### 3.1.1. Influence of Injection-Production Cycle and Differential Pressure on Sand Cementation

The formation rock is formed by sand cementation. During the gas-solid coupling process, the cementation between sand particles will be partially broken due to the action of alternating load, resulting in the cemented skeleton sand becoming free sand [18,19], which will affect the mechanical properties of formation rock. Therefore, the influence of injection-production cycle and differential pressure on core sand cementation due to gas-solid coupling is analyzed from the micro perspective.

The characteristics of bond contact crack between particles in rock core under alternating load in different cycles are shown in Figure 4. The red part shows the bond contact crack of core after loading core for 1, 30, and 60 cycles. It can be clearly seen that with the increase of alternating load loading cycle, the number and distribution range of bond contact cracks in rock core gradually increase, and the increase is concentrated in the area with dense distribution of original rock cracks. The reason is that the concentrated stress will be generated in the area with dense crack distribution, and the distribution of bond

contact crack is mainly controlled by the original crack distribution. Bond contact crack is most likely to occur near the area with dense original crack distribution.

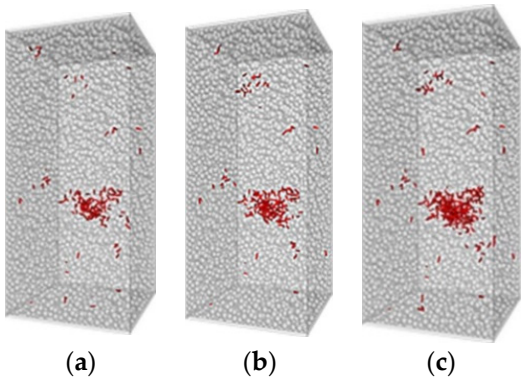


**Figure 4.** Bond contact crack characteristics at different stages of alternating load loading. (**a**) Load 1 cycle. (**b**) Load 30 cycles. (**c**) Load 60 cycles.

The statistical results of bond contact crack in rock core in each loading cycle of alternating load are shown in Figure 5. It can be seen that the number of bond contact cracks gradually increases with the increase of loading cycle of alternating load. In addition, the bond contact crack in rock core in the first cycle of alternating load is the most serious. The number of bond contact cracks in the first five cycles exceeds half of the total number of bond contact cracks in the whole alternating load loading process. The bond contact crack in the early stage of alternating load is much more serious than that in the late stage of alternating load. The reason is that the internal structure of the core is heterogeneous, and the external force borne by the particles in each area is different under pressure. In the first cycle loading stage, the external force borne by the bonding contact between the local particles of the core is large. When the external force exceeds the tensile or shear strength limit of the bonding contact, the bonding contact will break, which is a rigid tensile or shear failure. In the following 59 loading cycles, the external force borne by the bond contact between particles gradually increases. When the external force exceeds the bond contact strength limit, the bond contact will break, which is fatigue damage.

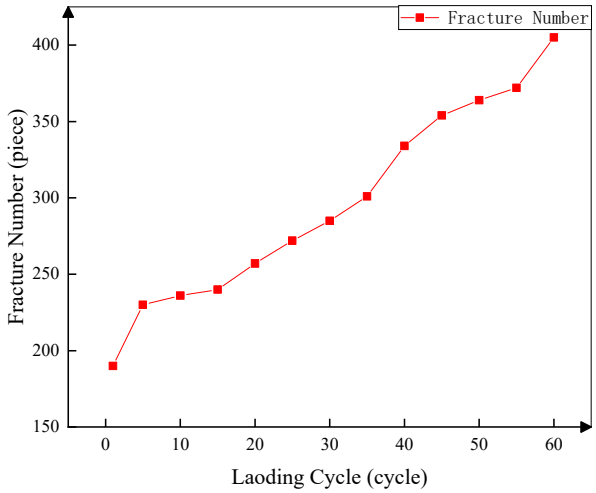


**Figure 5.** Bond contact crack in each loading cycle.

### 3.1.2. Influence of Injection-Production Cycle and Differential Pressure on Crack Evolution

There is a complex original crack network in the formation of the gas storage. New cracks may be generated in the formation due to gas-solid coupling during the cyclic injection and production of injection-production wells. The emergence of new cracks

will have a great impact on the overall mechanical properties of the formation of the gas storage. Therefore, the influence of injection-production cycle and differential pressure on the evolution and development of cracks in core under gas-solid coupling is studied from the micro perspective of particle flow dispersion element.

The comparison of the distribution and evolution characteristics of new cracks in the rock core at each stage of alternating load loading is shown in Figure 6. The blue ellipse and yellow box areas can be divided into two types of new crack characteristics for analysis. Compared with the yellow box area in Figure 6, it is found that with the increase of loading cycle, some cracks will extend outward along the edge, and the distribution range of cracks in rock core will increase slightly. The blue oval area in Figure 6 shows that a few cracks in the core will be partially or even completely closed during loading. On the whole, the crack development in the early stage of loading is more complex than that in the later stage.

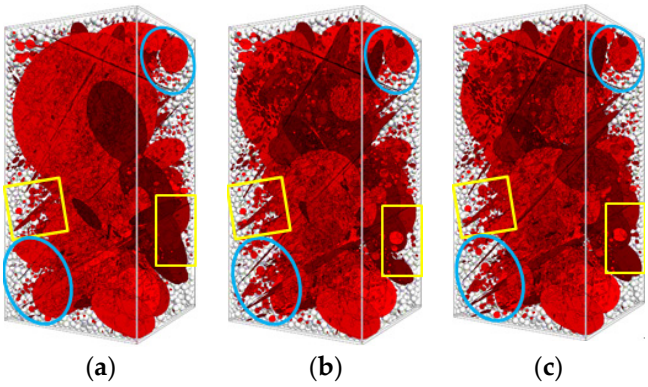


**Figure 6.** Crack development characteristics at different stages of alternating load loading. (**a**) Load 1 cycle. (**b**) Load 30 cycles. (**c**) Load 60 cycles.

According to the statistics of the number and area of new cracks in the rock core in each alternating load loading cycle, as shown in Figure 7, it can be clearly seen that with the increase of alternating load loading cycle, the number of cracks in the rock core increases rapidly, then decreases slightly, and then increases slowly, while the crack area increases gradually and the increasing trend slows down.

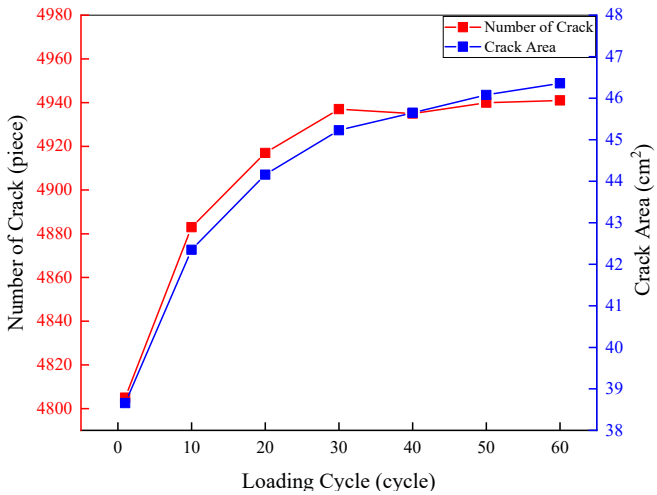


**Figure 7.** Crack development characteristics at different stages of alternating load loading.

By comprehensively analyzing the variation law of the number and area of new cracks, with the increase of alternating load loading cycle, it is found that the number and area of cracks increase rapidly in 1–30 cycles of alternating load loading. It is considered that the development characteristics of total cracks in this stage are mainly characterized

by the rapid initiation of cracks, and the increase of crack area is mainly caused by the increase of crack number; in 31–40 cycles of alternating load loading, the number of cracks decreases slightly and the crack area increases slowly. The reason is that the development characteristics of total cracks in this stage are mainly characterized by the outward extension of cracks along the edge and the mutual penetration and connection of multiple cracks. The decrease of crack number is caused by the mutual connection of multiple cracks into one crack, and the increase of crack area is mainly caused by the outward extension of cracks along the edge. The number and area of cracks increase slowly in 41–60 cycles of alternating load loading. The reason is that the crack development characteristics at this stage are mainly characterized by the slow extension of cracks along the edge and the slow initiation of secondary cracks. The increase of crack area is caused by the outward extension of cracks along the edge and the increase of the number of cracks.

### *3.2. Influence of Gas-Solid Coupling on Macro Mechanical Properties*

Firstly, keeping the confining pressure in the two principal stress directions of the numerical core loaded with alternating load in different injection-production cycles unchanged and then unload the axial loading stress to the same size as the confining pressure in the direction of horizontal minimum principal stress. Finally, the true triaxial compression numerical simulation experiment will be carried out on the numerical core. According to the stress–strain data, the elastic deformation parameters of core in each injection-production cycle are calculated to analyze the influence of injection-production cycle and differential pressure on the elastic deformation parameters of core sample under gas-solid coupling action.

#### 3.2.1. Influence of Injection-Production Cycle and Differential Pressure on Elastic Modulus

After the true triaxial compression numerical simulation experiment is carried out on the numerical cores with different injection-production cycles under alternating load, the elastic modulus under different injection-production cycles and differential pressure is calculated according to the axial stress–strain data, and then the relationship between the elastic modulus ratio and injection-production cycle and differential pressure will be finally obtained.

According to the experimental test results, as shown in Figure 8 (dots are simulation results and curves are trend lines), the change of elastic modulus ratio of each stress amplitude is analyzed. It can be clearly seen that under each injection-production cycle, the elastic modulus ratio gradually decreases with the increase of injection-production cycle, and the decrease amplitude gradually slows down. Moreover, the higher the injection-production differential pressure, the greater the decrease of elastic modulus ratio with the increase of injection-production cycle. The reason is that after the injection-production differential pressure increases, the number of bond contact cracks and crack area in the numerical core increases under the same injection-production cycle, the overall strength of the numerical core decreases, the ability of the numerical core to resist deformation under the action of external force decreases, and the axial deformation of the numerical core is greater at the same stress level. Therefore, the elastic modulus of the numerical core decreases with the increase of injection-production differential pressure, and the greater the injection-production cycle, the greater the overall strength decrease of the numerical core. Therefore, the more the injection-production cycle, the greater the decrease of elastic modulus and there is a good power function relationship between the elastic modulus ratio and the injection-production pressure drop in this area. The power function can be used to describe the relationship between the elastic modulus ratio and the injection-production pressure drop in the change process of a single injection-production pressure drop, that is:

$$K_E = a \triangle P^{-b} \quad (1)$$

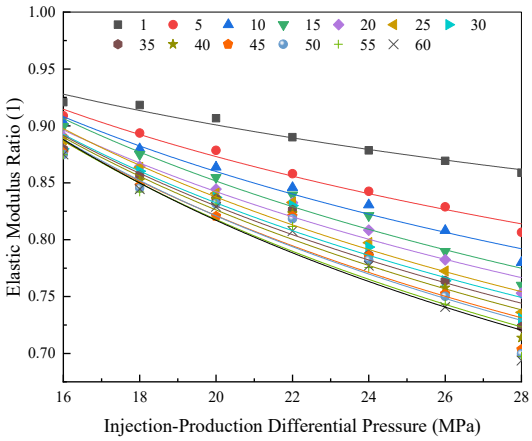


**Figure 8.** Elastic modulus ratio changes under different injection-production differential pressure and cycle.

Fitting parameters a and b also have a good power function relationship with the number of injection-production cycles, so the relationship model between fitting parameters a and b and the number of injection-production cycles can be established by using power function regression analysis, respectively, as shown in Figure 9. Then, the relationship model between the fitting parameters a and b under each injection-production cycle and the number of injection-production cycles of the gas storage is:

$$a = -0.3062 + 0.31628n^{0.33989} \quad (2)$$

$$b = 1.96755 - 0.97173n^{0.16973} \quad (3)$$

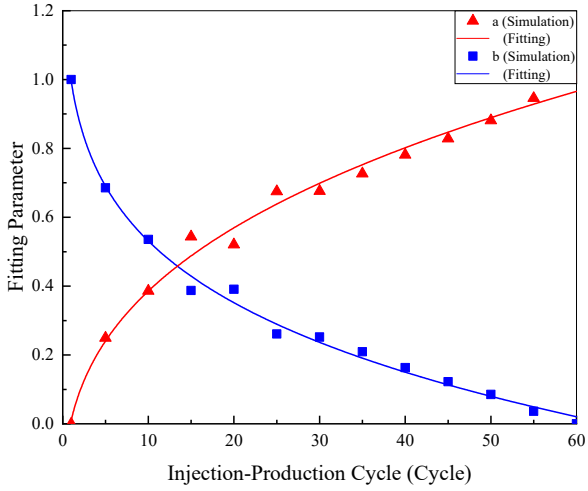


**Figure 9.** Fitting parameters (a and b) change with cycle increase range.

Substituting Equations (2) and (3) into Equation (1), the elastic modulus of rock under injection-production pressure drop in any operation cycle of gas storage due to gas-solid coupling can be calculated, namely:

$$E = E_i K_E = K_i \left[ \left( -0.3062 + 0.31628n^{0.33989} \right) \triangle P^{1.96755 - 0.97173n^{0.16973}} \right] \quad (4)$$

where E is the elastic modulus of formation rock, MPa; $E_i$ is the original elastic modulus of formation rock, MPa; $K_E$ is the relative elastic modulus ratio, dimensionless; $\triangle P$ is the injection-production pressure drop, MPa; n is the injection-production cycle, cycle; a and b are the fitting parameters.

3.2.2. Influence of Injection-Production Cycle and Differential Pressure on Poisson's Ratio

After performing true triaxial compression numerical simulation experiments on numerical cores with different injection-production cycles, the Poisson's ratio with each injection-production cycle under gas-solid coupling is calculated according to the axial strain and transverse strain data. However, the true triaxial model has transverse strains in the two directions of horizontal minimum and maximum principal stress, so the Poisson's ratios in the two directions can be calculated respectively. The ratio of the Poisson's ratio in each injection-production cycle to the initial Poisson's ratio of the numerical core is recorded as the relative Poisson's ratio. The relationship between the relative Poisson's ratio in the direction of horizontal minimum and maximum principal stress and the injection-production cycle, injection-production differential pressure is respectively obtained, as shown in Figure 10 (dots are simulation results and curves are trend lines) and Figure 11.

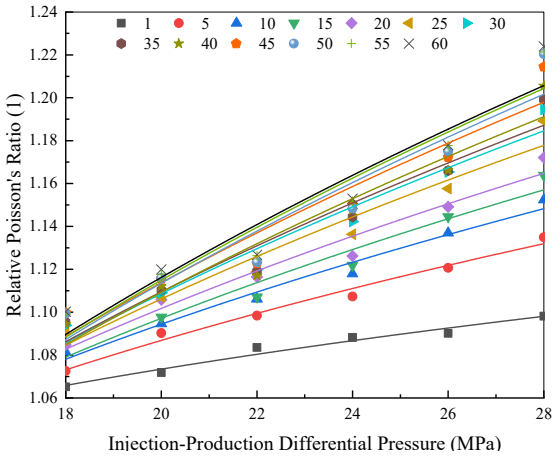


**Figure 10.** Relative Poisson's ratio changes of minimum principal stress direction under different injection-production differential pressure and cycle.

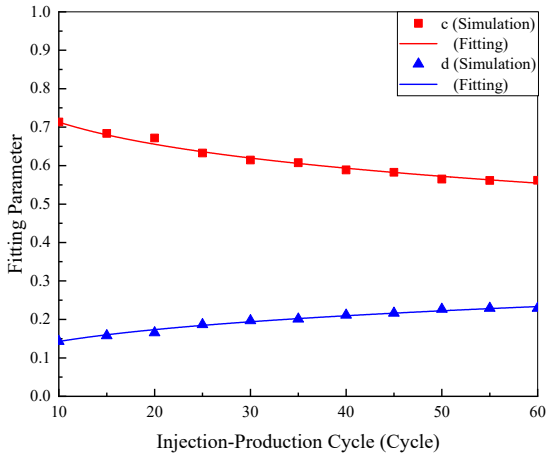


**Figure 11.** Fitting parameters (c and d) change with cycle increase range.

As shown in Figure 10, according to the analysis of experimental test results, in the direction of horizontal minimum principal stress, the relative Poisson's ratio under each injection-production differential pressure gradually increases with the increase of injection-production cycle, and the increasing range gradually slows down. When the injection-production cycle is the same, with the increase of injection-production differential pressure, the relative Poisson's ratio of gradually increases, and generally the more the injection-production cycle is, the greater the increase of relative Poisson's ratio is. On the one hand, the reason is that after the injection-production differential pressure increases, the number of bond contact cracks and crack area in the numerical core increase at the

same injection -production cycle, the overall strength of the numerical core decreases, the ability of the numerical core to resist deformation under the action of external force decreases, and the transverse deformation and axial deformation of the numerical core increase due to gas-solid coupling at the same stress level. On the other hand, the unbonded contact and new cracks produced by bonded contact crack cannot bear tensile stress but compressive stress, resulting in the increase of transverse deformation of numerical core at the same stress level is greater than that of axial deformation. Therefore, with the increase of injection-production differential pressure, the Poisson's ratio in the direction of horizontal minimum principal stress of numerical core increases, while the more injection-production cycles, the greater the overall strength decline of numerical core, and the more injection-production cycles, the greater the increase of Poisson's ratio in the direction of horizontal minimum principal stress of numerical core. Secondly, there is a good power function relationship between the relative Poisson's ratio in the direction of the minimum principal stress and the injection-production pressure drop in this area. The power function can be used to describe the relationship between the relative Poisson's ratio in the direction of the minimum principal stress and the injection-production pressure drop in the change process of a single injection-production pressure drop, that is:

$$K_v^{min} = a \triangle P^{-b} \tag{5}$$

Fitting parameters c and d have a good power function relationship with the number of injection-production cycles, so the relationship model between fitting parameters c and d and the number of injection-production cycles can be established by using power function regression analysis, respectively, as shown in Figure 11. Then, the relationship model between the fitting parameters c and d under each injection-production cycle and the number of injection-production cycles of the gas storage is:

$$c = 1.41174 - 0.53704n^{0.11422} \tag{6}$$

$$d = -0.03954 + 0.10824n^{0.22596} \tag{7}$$

Substituting Equations (6) and (7) into Equation (5), Poisson's ratio in the direction of minimum principal stress of rock under injection-production pressure drop in any operation cycle of gas storage due to gas-solid coupling can be calculated, namely:

$$v = v_i K_v^{min} = v_i \left[ \left( -1.41174 - 0.53704n^{0.11422} \right) \triangle P^{0.03954 - 0.10824n^{0.22596}} \right] \tag{8}$$

where v is Poisson's ratio of horizontal minimum principal stress direction of the formation rock, dimensionless; $v_i$ is the original Poisson's ratio of formation rock, dimensionless; $K_v^{min}$ is the relative Poisson's ratio in the direction of horizontal minimum principal stress, dimensionless; $\triangle P$ is the injection-production pressure drop, MPa; n is the injection-production cycle, cycle; c and d are the fitting parameters.

As shown in Figure 12 (dots are simulation results and curves are trend lines), according to the experimental test results, in the direction of horizontal maximum principal stress, the relative Poisson's ratio under each injection-production differential pressure gradually increases with the increase of injection-production cycle, and the increase amplitude gradually slows down. Moreover, the higher the injection-production differential pressure, the greater the increase of relative Poisson's ratio with the increase of injection-production cycle. In addition, under the condition of the same injection-production cycle, the relative Poisson's ratio gradually increases with the increase of injection-production differential pressure, and the increase difference of relative Poisson's ratio in each injection-production cycle with the increase of injection-production differential pressure is not obvious. On the one hand, with the increase of injection-production differential pressure, the increase mechanism of Poisson's ratio in the two horizontal principal stress directions is the same, and the difference of confining pressure leads to the increase of Poisson's ratio in the direc-

tion of maximum principal stress is less than that in the direction of minimum principal stress. On the other hand, with the increase of injection-production differential pressure, the increase mechanism of Poisson's ratio in the two horizontal principal stress directions is the same. The difference of confining pressure leading to the increase of Poisson's ratio in the direction of maximum principal stress is less than that in the direction of minimum principal stress. Then, the relative Poisson's ratio of the maximum principal stress direction in this area has a good logarithmic function relationship with the injection-production cycle. The logarithmic function can be used to describe the relationship between the relative Poisson's ratio of the maximum principal stress direction and the injection-production cycle in the change process of a single injection-production cycle, that is:

$$K_v^{max} = e\ln(n) + f \tag{9}$$

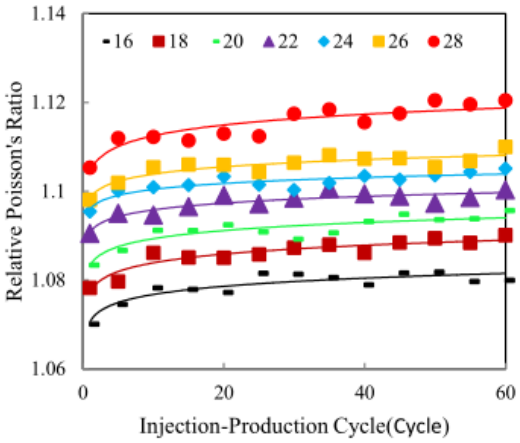


**Figure 12.** Relative Poisson's ratio changes of maximum principal stress direction under different injection-production differential pressure and cycle.

Firstly, regression analysis is used for fitting parameters e and f respectively, and the relationship model between fitting parameters e and e and injection-production cycle number is established, as shown in Figure 13. Then, the relationship model between the fitting parameters e and f under each injection-production pressure drop and the injection-production pressure drop of the gas storage is:

$$e = -38.42 + 5.83 \triangle P - 0.3 \triangle P^2 - 0.0046 \triangle P^3 \tag{10}$$

$$f = 1.03 + 0.003 \triangle P \tag{11}$$

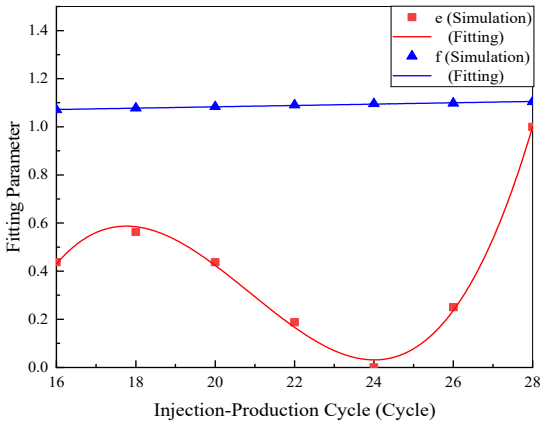


**Figure 13.** Fitting parameters (e and f) change with cycle increase range.

Substituting Equations (10) and (11) into Equation (9), the relative Poisson's ratio in the direction of the maximum principal stress of rock under injection-production pressure drop in any operation cycle of gas storage due to gas-solid coupling can be calculated, namely:

$$v = v_i K_v^{max} = \left(-38.42 + 5.83 \triangle P - 0.3 \triangle P^2 - 0.0046 \triangle P^3\right) \ln(n) + 1.03 + 0.003 \triangle P \quad (12)$$

where v is the Poisson's ratio in the direction of the maximum principal stress of the formation rock, dimensionless; $v_i$ is the Poisson's ratio of the original maximum principal stress direction of the formation rock; $K_v^{max}$ is the relative Poisson's ratio in the direction of maximum principal stress, dimensionless; △P is the injection-production pressure drop, MPa; n is the injection-production cycle, cycle; e, f is the fitting parameter.

3.2.3. Influence of Injection-Production Cycle and Differential Pressure on Cohesion Ratio

After three groups of true triaxial compression numerical simulation experiments with different confining pressures under gas-solid coupling are carried out on numerical cores with different injection-production cycles. Then, the Mohr strength envelope of numerical cores is obtained according to the compression failure strength data of three groups of numerical cores under different confining pressures. Finally, the cohesion is obtained from the longitudinal intercept of the Mohr strength envelope. Among them, the cohesion in each injection-production cycle is dimensionless into cohesion ratio, and lastly the relationship between cohesion ratio and injection-production cycle and injection-production differential pressure is shown in Figure 14 (dots are simulation results and curves are trend lines).

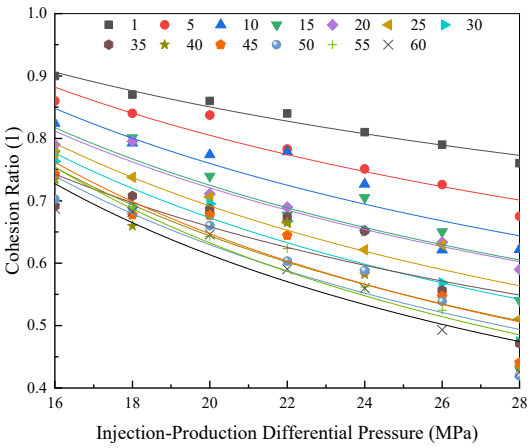


**Figure 14.** Cohesion ratio changes under different injection-production differential pressure and cycle.

A as shown in Figure 14, according to the analysis of the experimental test results, under each injection-production differential pressure, the cohesion ratio gradually decreases with the increase of injection-production cycle, and the reduction range gradually slows down. Moreover, the higher the injection-production differential pressure, the greater the decrease of cohesion ratio with the increase of injection-production cycle. Under the condition of the same injection-production cycle, with the increase of injection-production differential pressure, the cohesion ratio decreases gradually, and the more injection-production cycles, the greater the decline of cohesion ratio. On the one hand, the reason is that with the injection-production differential pressure increases and the effect of gas-solid coupling, the number of bond contact cracks and crack area in the numerical core increases under the same injection-production cycle, the overall strength of the numerical core decreases. The unbonded contact and new cracks generated by the bond contact crack in the numerical core cannot bear the tensile stress, resulting in the loosening of local particle system. Therefore, the injection-production differential pressure increases and the cohesion decreases. On the other hand, the more the injection-production cycle is, the greater the overall strength decline of the numerical core is. Therefore, the more injection-production cycles, the

greater the decline of cohesion. Additionally, there is a good power function relationship between the cohesion ratio and the injection-production pressure drop in this area. The power function can be used to describe the relationship between the cohesion ratio and the injection-production pressure drop in the change process of a single injection-production pressure drop, namely:

$$K_c = g \triangle P^{-h} \tag{13}$$

Fitting parameters g and h have a good power function relationship with the number of injection-production cycles, so the relationship model between fitting parameters g, h and the number of injection-production cycles can be established by using power function regression analysis, respectively, as shown in Figure 15. Then, the relationship model between the fitting parameters g and h under each injection-production cycle and the number of injection-production cycles of the gas storage is:

$$g = -0.03318 + 0.05422n^{0.70366} \tag{14}$$

$$h = 1.28067 - 0.28935n^{0.36088} \tag{15}$$

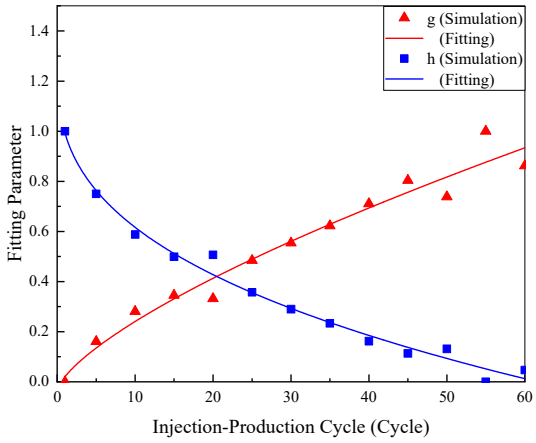


**Figure 15.** Fitting parameters (g and h) change with stress increase range.

Substituting Equations (14) and (15) into Equation (13), the cohesion of rock under injection-production pressure drop in any operation cycle of gas storage due to gas-solid coupling can be calculated, namely:

$$c = c_i K_c = c_i \left[ \left( -0.3062 + 0.31628n^{0.33989} \right) \triangle P^{1.96755 - 0.97173n^{0.16973}} \right] \tag{16}$$

where c is the cohesion of formation rock, MPa; $c_i$ is the original cohesion of formation rock, MPa; $K_c$ is the cohesion ratio, dimensionless; $\triangle P$ is the injection-production pressure drop, MPa; n is the injection-production cycle, cycle; g and h are the fitting parameters.

### 3.2.4. Influence of Injection-Production Cycle and Differential Pressure on Internal Friction Angle

After three groups of true triaxial compression numerical simulation experiments with different confining pressures are carried out for numerical cores loaded with alternating load in different cycles. Firstly, the Mohr strength envelope of numerical cores is obtained according to the compression failure strength data of numerical cores under three groups of confining pressures. Then, the internal friction angle will be obtained from the angle between Mohr strength envelope and transverse axis. Among them, the internal friction angle of numerical cores in each injection-production cycle is dimensionless into the internal friction angle ratio. Finally, the relationship between the internal friction angle ratio and injection-production cycle and differential pressure can be obtained, as shown in Figure 16 (dots are simulation results and curves are trend lines).

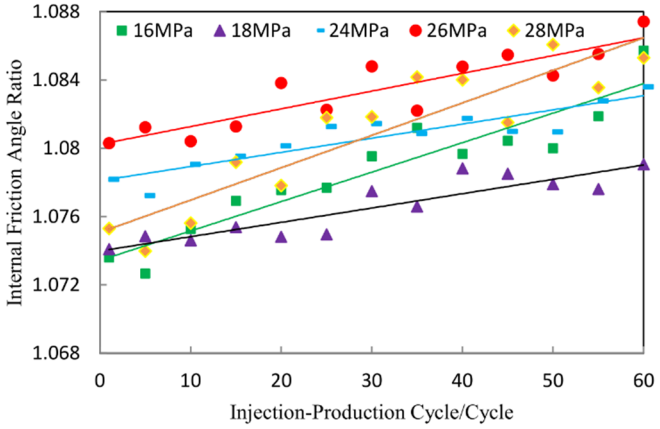


**Figure 16.** Internal friction angle ratio changes under different injection-production differential pressure and cycle.

Fitting the internal friction angle ratio in Figure 16 with the numerical simulation data of injection-production cycle, the following relationship is obtained:

$$k_\varphi = \lambda e^{\beta n} \tag{17}$$

Fitting the internal friction angle ratio under each stress amplitude in Figure 16 with the data of injection-production cycle to obtain the fitting parameters λ and β The variation with the increase of injection-production cycle is shown in Figure 17. It can be seen that the fitting parameters in formula (18) and formula (19) increase with the increase of injection-production cycle λ decrease and then increase, β gradually increase and then decrease, namely:

$$\lambda = 0.02643\Delta p^2 - 1.14881\Delta p + 12.556 \tag{18}$$

$$\beta = -0.00431\Delta p^3 + 0.2724\Delta p^2 - 5.547\Delta p + 36.75 \tag{19}$$

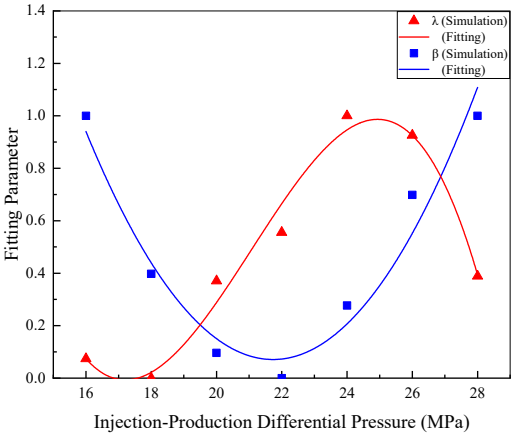


**Figure 17.** Fitting parameters (λ and β) change with stress increase range.

Substituting Equations (18) and (19) into Equation (17), the internal friction angle of rock under injection-production pressure drop in any operation cycle of gas storage due to gas-solid coupling can be calculated, namely:

$$\varphi = \varphi_i K_\varphi = \varphi_i \left(0.02643\Delta p^2 - 1.14881\Delta p + 12.556\right) e^{(-0.00431\Delta p^3 + 0.2724\Delta p^2 - 5.547\Delta p + 36.75)n} \tag{20}$$

where φ is the internal friction angle of formation rock, (°); $\varphi_i$ is the original internal friction angle of formation rock, (°); $K_\varphi$ is the internal friction angle ratio, dimensionless; Δp is the injection-production pressure drop, MPa; n is the loading cycle of alternating load, cycle; λ and β are fitting parameters.

## 4. Discussion

### *4.1. Dynamic Prediction Model of Critical Production Pressure Drop under Gas-Solid Coupling in Gas Storage*

The mechanical properties of formation rock will change with the increase of injection-production cycle in the process of gas-solid coupling in gas storage, which leads to the change of critical production pressure drop of gas storage injection-production wells with the increase of injection-production cycle. According to the influence law of alternating load on numerical core mechanical parameters, the relationship between critical production pressure drop of injection-production wells in gas storage and injection-production cycle and operating pressure is established, as shown in Equation (21). Therefore, given the original parameters of reservoir formation rocks, combining Equations (4), (8), (12), (16) and (20), the above method can be used to calculate the critical production pressure drop of gas storage under any injection-production cycle and differential pressure due to gas-solid coupling action, namely:

$$\triangle p_c = \frac{2\left[\frac{2v}{1-v}\alpha - 1\right]P_r - 2c\tan\varphi + \frac{2v}{1-v}P_0}{\frac{2v}{1-v}\alpha - 2} \tag{21}$$

where $\triangle p_c$ is the critical production differential drop, MPa; c is the cohesion of formation rock, MPa; φ Is the internal friction angle of formation rock, (°); $P_r$ is the boundary pressure of oil and gas reservoir, MPa; v is Poisson's ratio of stratum rock, dimensionless; $P_0$ is the vertical in-situ stress of the formation, MPa; $\alpha$ is the Biot coefficient of formation ($\alpha = 1 - \frac{E}{3(1-2v)} \times 10^{-5}$), dimensionless; E is the elastic modulus of formation rock, MPa.

### *4.2. Comparison and Analysis of Prediction Results of Dynamic Prediction Models for Critical Production Pressure Drop of Gas Storage*

At present, the prediction model of critical production differential drop is established according to the one-way flow operation mode of oil and gas reservoirs, and the critical production differential drop is predicted using the static rock mechanics parameters of the formation that only represent the physical property state of the reservoir at the initial stage of development. In fact, the mechanical properties of formation rock will change dynamically under the effect of gas-solid coupling. Therefore, the dynamic and static models considering the gas-solid coupling and not considering the gas-solid coupling are used to compare and analyze the prediction results of the two models. It is known that the injection-production well depth of a gas storage in the west is 3557.7 m, the original formation pore pressure is 33.96 MPa, and the variation range of formation pore pressure during the production and operation of the gas storage is 18–34 MPa. See Table 2 for specific block physical parameters and Figure 18 for the calculation results.

**Table 2.** Physical parameters of reservoir.

| Formation Parameter | $E_i$/MPa | $v_i$/(N·m$^{-1}$) | $c_i$/MPa | $\varphi_i$/(°) |
|---|---|---|---|---|
| Values | 9.2 | 7.0 | 0.4 | 12.0 |

Figure 18 shows the model prediction results of 60 cycles of cyclic injection and production in the gas storage under the conditions of formation pressures of 18 MPa, 22 MPa, 26 MPa, 30 MPa, and 34 MPa, respectively, during production and operation. It can be seen that the prediction results of the dynamic and static critical production differential drop prediction models are obviously different. The difference between the prediction results of the static model and the dynamic model gradually increases with the increase of the injection-production cycle. Under the conditions of formation pressure, the critical production differential drop of the injection-production wells in the gas storage decreases with the increase of the injection-production cycle, and the change trend is basically the same. When the formation pressure in the 60th cycle of circulating injection production is

30 MPa, the critical production differential drop of injection-production wells predicted by the dynamic model is 10.34 MPa lower than that predicted by the static model, a year-on-year decrease of 51.23%. This shows that the gas solid coupling effect is very obvious during the injection and production operation of the underground natural gas storage, and the prediction results of the static model without considering the gas solid coupling cooperation are conservative and cannot be applied to the full life cycle of the gas storage.

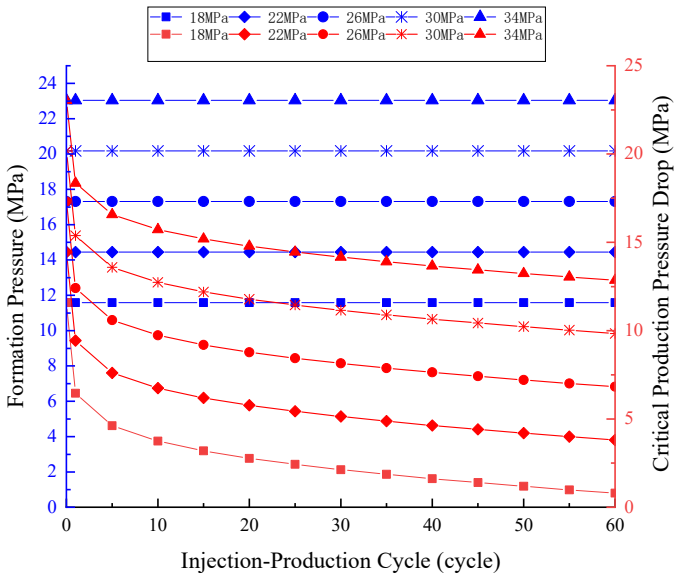


**Figure 18.** Comparison of prediction results between dynamic model and static model.

## 5. Conclusions

The results show that the number of bond contact fractures and micro-fractures in the model increases gradually with the increase of injection-production cycle due to gas-solid coupling. The elastic modulus ratio and cohesion ratio decrease gradually, and the higher the injection-production pressure difference, the greater the decline. At the same time, with the increase of injection-production cycle, Poisson's ratio gradually increases, and the higher the injection-production pressure difference, the greater the increase. The angle ratio of internal friction increases linearly after increasing greatly at the initial stage. According to the influence law, the relationship model between critical production pressure difference, injection-production cycle and pressure difference of injection-production wells in gas storage under the action of gas-solid coupling is established, which is used to predict the dynamic performance of critical production pressure drop of injection-production wells in the whole life cycle of gas storage.

**Author Contributions:** Conceptualization, G.L.; data curation, L.R.; formal analysis, Y.W.; investigation, Y.Z.; methodology, T.L.; resources, T.L.; supervision, Y.S.; visualization, M.L.; writing—original draft, Y.S.; writing—review and editing, M.L. All authors have read and agreed to the published version of the manuscript.

**Funding:** This research received no external funding.

**Data Availability Statement:** Not applicable.

**Conflicts of Interest:** The authors declare no conflict of interest.

## References

1. Zheng, D.; Xu, H.; Wang, J.; Sun, J.; Zhao, K.; Li, C.; Shi, L.; Tang, L. Key technologies for construction and evaluation of gas reservoir type gas storage. *Pet. Explor. Dev.* **2017**, *44*, 794–801. [CrossRef]
2. Ding, G.; Wei, H. Review and prospect of underground gas storage construction in China in 20 years. *Oil Gas Storage Transp.* **2020**, *39*, 25–31.

3. Xu, H.; Dong, H.; Lv, J.; Wu, G.; Wang, J.; Zhao, K.; Li, C. Reasonable injection allocation method at the initial stage of operation of water invasion depleted gas reservoir gas storage. *Nat. Gas Ind.* **2017**, *37*, 93–95.
4. Yin, H.; Chen, J.; Lan, Y.; Lan, Y.; Liu, Z. Technical development status and Enlightenment of typical gas storage in North America. *Oil Gas Storage Transp.* **2013**, *32*, 815–818.
5. Ma, X.; Zheng, D.; Shen, R.; Wang, C.; Luo, J.; Sun, J. Key technology and practice of building gas reservoir with complex geological conditions in China. *Pet. Explor. Dev.* **2018**, *45*, 489–499. [CrossRef]
6. Li, X.; Zhang, Q.; Li, H. Grain-based discrete element method (GB-DEM) modeling of multi-scale fracturing in rocks under dynamic loading. *Rock Mech. Rock Eng.* **2018**, *51*, 3785–3817. [CrossRef]
7. Erarslan, N. Microstructural investigation of subcritical crack propagation and crack process zone (FPZ) by the reduction of rock crack toughness under cyclic loading. *Eng. Geol.* **2016**, *208*, 181–190. [CrossRef]
8. Oluyemi, G.F.; Oyeneyin, M.B. Analytical critical drawdown (CDD) failure model for real time sanding potential prediction based on Hoek and Brown failure criterion. *J. Pet. Gas Eng.* **2010**, *1*, 16–25.
9. Adeyanju, O.; Oyekunle, L. A new model for the prediction of real time critical drawdown sand failure in petroleum reservoirs. *Pet. Sci. Technol.* **2014**, *32*, 140–149. [CrossRef]
10. Ge, X.; Ren, J.; Pu, Y.; Ma, W.; Zhu, Y. Preliminary study on CT mesoscopic analysis of fatigue damage propagation law of rock. *Acta Geotech. Eng.* **2001**, *23*, 191–195.
11. Nguyen, N.H.T.; Bui, H.H.; Kodikara, J.; Arooran, S.; Darve, F. A discrete element modeling approach for fatigue damage growth in cemented materials. *Int. J. Plast.* **2019**, *112*, 68–88. [CrossRef]
12. Liu, X.; Liang, L.; Yang, L.; Zeng, X.; Cao, J.; Long, Y.; Liu, H. Influence of branch well configuration on critical production pressure difference in unconsolidated sandstone reservoir. *J. Pet. Sci.* **2011**, *32*, 717–721.
13. Arora, K.; Chakraborty, T.; Rao, K.S. Experimental study on stiffness degradation of rock under uniaxial cyclic sinusoidal compression loading. *Rock Mech. Rock Eng.* **2019**, *52*, 4785–4797. [CrossRef]
14. Li, S.; Chen, Y. Optimization of drawdown pressure about the ultra-deep cracked carbonate reservoir. In *SPE Kingdom of Saudi Arabia Annual Technical Symposium and Exhibition*; SPE192394; OnePetro: Richardson, TX, USA, 2018.
15. Jiang, M.; Zhang, N.; Shen, Z.; Chen, H. Discrete element analysis of crack propagation mechanism of cracked rock mass under uniaxial compression. *Rock Soil Mech.* **2015**, *36*, 3294–3298.
16. Sun, X.; Liu, C.; Xve, S. Application of mixed finite element and discrete element method in crack propagation. *J. China Univ. Pet.* **2013**, *37*, 126–136.
17. Zhang, C.; Tu, S.; Bai, Q. Evaluation of pore size and distribution impacts on uniaxial compressive strength of lithologic rock. *Arab. J. Sci. Eng.* **2018**, *43*, 1236–1244. [CrossRef]
18. Hu, W. *Study on Mechanical Characteristics of Jointed Rock Mass Based on Smooth Joint Model*; Wuhan University: Wuhan, China, 2017; pp. 41–52.
19. Wang, T.; Zhao, H.; Li, K.; Gan, L.; Huo, Q. A seismic petrophysical model of shale considering complex pore structure. *J. China Univ. Pet.* **2019**, *43*, 45–55.